

Recent Advances in Long Pulse Divertor Operations on EAST

H.Y. Guo 1, 2), J. Li 1), G.-N. Luo 1), Z.W. Wu 1), S. Zhu 1), J.F. Chang 1), W. Gao 1), X. Gao 1), X.Z. Gong 1), Q.S. Hu 1), Q. Li 1), S.C. Liu 1), T.F. Ming 1), J. Ou 1), Y.J. Shi 1), B.N. Wan 1), D.S. Wang 1), H.Q. Wang 1), J. Wang 1), L. Wang 1), B.J. Xiao 1), G.S. Xu 1), Q. Xu 1), L. Zhang 1), W. Zhang 1), and the EAST Team 1)

1) Institute of Plasma Physics, Chinese Academy of Sciences, Hefei, P.R. China

2) Tri Alpha Energy, California, USA

E-mail contact of main author: hguo@trialphaenergy.com

Abstract. The first systematic assessment of divertor performance was made in the EAST superconducting tokamak for both single null (SN) and double null (DN) divertor configurations under Ohmic and L-mode plasma conditions. A strong in-out divertor asymmetry in particle and heat fluxes occurs for DN, favoring outer divertors, but is significantly reduced for SN. DN operation also leads to an up-down asymmetry with higher particle fluxes to the divertors with their ∇B drift toward the X-point. Reversing toroidal field direction shows a strong influence on the divertor asymmetries. In addition, divertor screening for carbon and neutrals have been investigated by injecting CH_4 and D_2 from various divertor locations, *i.e.*, inner divertor target, outer divertor target and private flux region. Furthermore, localized divertor puffing of Ar has been explored as a means to mitigate divertor asymmetry and reduce heat load at divertor target plates.

1. Introduction

The Experimental Advanced Superconducting Tokamak (EAST) was built to achieve higher power, long pulse operations over 1000s, thus providing a unique platform to address physics and engineering issues for next step fusion devices such as ITER [1, 2]. EAST has a flexible poloidal field control system to accommodate both single null (SN) and double null (DN) divertor configurations [3, 4]. The divertor geometry has adopted ITER-like vertical target structures with tightly fitted side baffles and a central dome in the private flux region to physically separate inboard/outboard divertor chamber and minimize the leakage of neutrals to the main chamber [5, 6]. The first experimental assessment of divertor performance was carried out on EAST during the first divertor physics campaign in the spring of 2009. We first studied the basic divertor plasma behavior under Ohmic mode operating conditions, and demonstrated the plasma detachment process. Comparisons were also made between SN and DN divertor configurations. To better understand divertor asymmetry and effect of classical drifts, we have carried out a dedicated field reversal experiment. In addition, we have assessed the performance of the newly installed divertor cryopump and investigated the effect of localized divertor puffing from various divertor locations, *i.e.*, inner divertor, outer divertor and private flux region, using a newly developed multipurpose gas fuelling system. Furthermore, we have carried out a preliminary study on divertor screening for carbon with methane puffing and radiative plasmas with argon injection. In this article, we present some highlights of these results and initial comparisons with B2/EIRENE modeling. More details can be found in Refs [7-11].

2. EAST First Wall Upgrade and Key Divertor/Edge Diagnostics

A significant upgrade was made on EAST in 2008 to convert the first wall (including both main vacuum chamber wall and divertor target plates) from stainless steel to SiC-coated, doped

graphite (1% B₄C, 2.5%Si, and 7.5%Ti), coupled with active water cooling, which limits the temperature rise at the graphite surface to 900 °C at the incident heat flux of 2 MW/m². SiC coating reduces erosion near strike points by suppressing chemical sputtering, and reduces carbon redeposition elsewhere by enhancing carbon reflection [10]. A new internal toroidal cryopump was installed in EAST under the lower outer divertor target plate with large pumping capacities, *i.e.*, 75 m³/s for D₂ and 107 m³/s for H₂ [11], to facilitate density control and impurity exhaust.

In addition, a multipurpose gas fuelling system was installed during the EAST first wall upgrade, with two gas puff locations at midplane on high field side and low field side, respectively, and six puff locations symmetrically distributed between upper and lower divertors at inner divertor, outer divertor and central dome in the private flux region, as shown in Fig. 1. This allows the introduction of D₂ and impurities, *e.g.*, CH₄ and Ar, from different poloidal positions to study divertor plasma and impurity behaviors, and actively control divertor asymmetry and power loading for high power, long pulse operations. An extensive set of divertor and edge plasma diagnostics were also installed or upgraded in EAST, including the following key diagnostics:

- *Langmuir probe system*: 222 divertor target embedded graphite probes, which can be configured as 74 triple probes or single probes [12], as shown in Fig. 1, and 2 sets of reciprocating probes inserted from the opposite sides of the mid-plane.
- *Spectroscopy*: 18-channel D_α and 18-channel CII/CIII, viewing the lower outboard divertor from the top of the machine; 2 arrays of 35-channel D_α, viewing the inner target and dome surfaces of both upper and lower divertors from the outer midplane through the in-vessel reflection mirrors (Fig. 1); 1 UV and Visible spectrometer with CCD (200-750nm), viewing the lower outer divertor; 2 sets of monochromators for CIII and OII lines and 1 interference filter for H_α monitor in the outer mid-plane; and 8-channel visible bremsstrahlung for Z_{eff}. A more detailed description of these diagnostics is given in Ref. [8]

3. Divertor Plasma Detachment for Long Pulse Operation

Long pulse diverted discharges well over 60 seconds have been achieved in EAST by lower hybrid current drive (LHCD) with advanced wall conditioning and active divertor pumping. The divertor power handling capability is presently limited to ~2 MW/m² on EAST. Thus, it must be operated under detachment conditions for high power, long pulse operations.

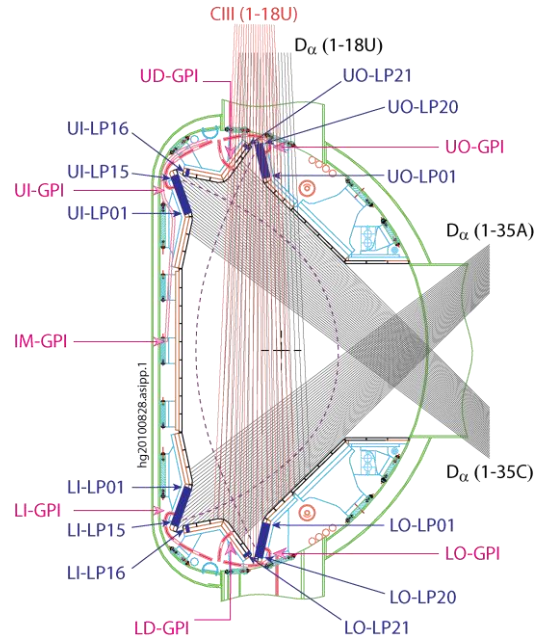


FIG. 1. Sketch of divertor gas puff locations and key divertor diagnostics on EAST. UO(I) – Upper Outboard (Inboard) divertor; LO(I) – Lower Outboard (Inboard) divertor; U(L)D – Upper (Lower) divertor Dome; IM – Inner Midplane; LP – Langmuir Probe; GPI – Gas Puff Inlet.

Detachment can be readily achieved in Ohmic and L-mode discharges by ramping up plasma density. Figure 2 shows the time evolution of a typical DN discharge during the density ramp-up with $I_p = 250$ kA, $B_T = 2$ T. As line averaged density, \bar{n}_e , increases, ion saturation, I_s , obtained from the divertor target Langmuir probe near strike points, first increases, then starts to roll over as \bar{n}_e further increases, finally decreases at sufficiently high densities as the plasma enters the detached regime where the volume recombination is important. Divertor neutral fluxes, as indicated by D_α , keep increasing with \bar{n}_e , but shows a tendency to saturate during detachment. The outer divertor plasma exhibits large amplitude broadband oscillations, while turbulence levels are significantly reduced in the inner divertor. In addition, there is a strong in-out divertor asymmetry in particle and heat fluxes, as seen by the target probes, favoring the outer divertor. Note that for the particular discharge shown in Fig. 2, the ion $\mathbf{B} \times \nabla B$ drift is directed toward the upper divertor, and only the upper divertor measurements are shown. Divertor asymmetry and effect of drifts in the divertor and edge plasmas are discussed in Section 5.

Detachment starts near the strike point, then expands further out along the divertor target, as plasma density rises. To illustrate this, Fig. 3 shows the profiles of ion saturation current density, j_s , electron density n_{et} and temperature, T_{et} , along the outer divertor target for the same discharge shown in Fig. 2, at two different times, *i.e.*, 3.7 s and 6.2 s, corresponding to attached and detached phases. As can be seen, both j_s and T_{et} are significantly reduced at detachment with $T_{et} \sim 3$ eV near the separatrix. Thus, the peak heat flux near the strike point on the target plate, $q_t \propto \gamma_t k T_{et} j_s / e$ [13], is greatly reduced at detachment. Here, γ_t is the heat transmission factor at the target plate with $\gamma_t \sim 8$, including both ion and electron contributions. Note, however, that at large heating power, the edge density needs to be sufficiently raised to achieve divertor detachment. This may not be compatible with high confinement modes and affects LHCD current drive efficiency. Furthermore, for the next phase of high power operations on EAST, the graphite tiles will be replaced by W coated Cu components to improve divertor power handling capability (up to 7~10 MW/m²). Therefore, highly radiative impurities such as Ar must be injected in divertor plasmas to promote detachment at lower densities through lack of intrinsic carbon radiation.

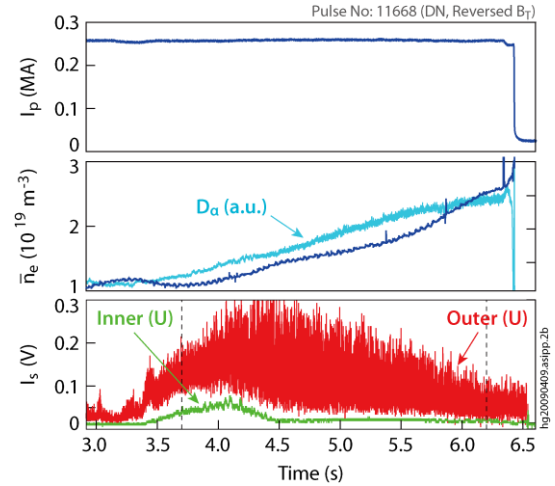


FIG. 2. Time evolution of an Ohmic double null discharge during a density ramp-up.

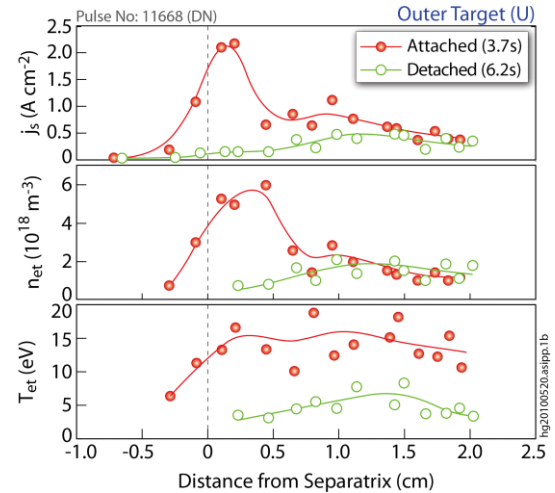


FIG. 3. Profiles of j_s , n_{et} , and T_{et} along the outer divertor target plate for shot 11668 during attached and detached phases.

4. Comparison between Single Null and Double Null Divertor Configurations

EAST has the capability to produce ITER-relevant SN divertor configuration, as well as DN divertor configuration, thus allowing exploration of a wide range of magnetic configurations for ITER and DEMO under steady-state operating conditions. The first comparison was made between SN and DN in Ohmic discharges during the first EAST divertor physics campaign. Figure 4 shows the time evolution of two density ramp-up discharges with $I_p = 250$ kA, $B_T = 2$ T (clockwise, with $\mathbf{B} \times \nabla B$ drift toward the lower X-point) for SN and DN, respectively. It can be seen that for a given density, particle fluxes to outer divertor targets appear to be comparable between SN and DN cases, as indicated by j_s obtained from Langmuir probes near the strike points at lower divertor targets (Note that j_s is not balanced between upper and lower divertors, to be discussed in Section 5), as observed in DIII-D [14, 15]. However, DN operation leads to a strong in-out divertor asymmetry with a much lower particle flux at the inner divertor target. This suggests a significantly lower particle loss through the inboard separatrix. In contrast, the divertor asymmetry is reduced for SN, possibly due to fast parallel transport along SOL. Strong turbulent fluctuations are present in the outer divertor for both DN and SN, most likely due to enhanced turbulence on the outboard side associated with bad curvature [6], which, at least in part, contributes to the higher particle loss through the outboard separatrix. In contrast, turbulence levels are significantly reduced at the inner target, especially for DN.

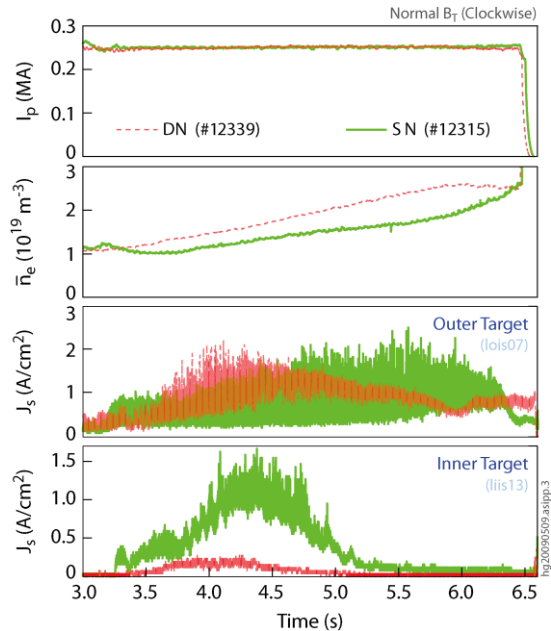


FIG. 4. Time evolution of two comparable SN and DN discharges with density ramp-up. The data shown are plasma current, I_p , line averaged electron density, \bar{n}_e , and ion saturation current density, j_s , from the target Langmuir probes near outer and inner strike points, respectively.

5. Effect of Field Reversal

Divertor asymmetry in particle and power fluxes is a critical issue for the design and operation of next-step higher powered long pulse tokamak devices such as ITER. Although the underlying mechanism for divertor asymmetry is still not fully understood, classical drifts appear to play an important role [16]. In the presence of steady electric and magnetic fields, basic single particle guiding-center drifts are the $\mathbf{E} \times \mathbf{B}$ and $\mathbf{B} \times \nabla B$ drifts (including both ∇B and curvature drifts). All classical drifts are influenced by the direction of the magnetic field. For the normal B_T direction, which is defined as that for which the $\mathbf{B} \times \nabla B$ drift is directed toward the X-point at the bottom, the power flux is larger at the outer divertor target than at the inner divertor target, leading to an intrinsic in-out divertor asymmetry [6]. For DN and near DN divertor configurations, the in-out divertor asymmetry is also affected by the divertor magnetic balance [14, 15], which is usually characterized by the distance between primary and secondary separatrices, defined as $dR_{\text{sep}} = R_L - R_U$, where R_L and R_U are the lower and upper separatrix radii mapped to the outer midplane. It

is found that even a well balanced double null divertor configuration ($dR_{\text{sep}} = 0$) still exhibits an up-down divertor asymmetry, thus corroborating the importance of classical drifts.

To investigate the effect of classical drifts on divertor asymmetry, a series of dedicated experiments were conducted in EAST for both DN and SN configurations with normal and reversed B_T directions. Figure 5 compares the ion fluxes, as represented by j_s , to the outer divertor targets between two Ohmic-mode density ramp-up discharges for the DN divertor configuration with different B_T directions, *i.e.*, shot 12339 with normal B_T and shot 11668 with reversed B_T ; here, only the j_s distributions on the outer targets are shown, as j_s at inner divertor targets has very small amplitudes throughout both discharges (see Figs 2,

4). As can be seen, for the normal B_T case, more particles go to the lower divertor target, *i.e.*, in the ion $\mathbf{B} \times \nabla B$ direction. Reversing the B_T direction appears to reverse the imbalances between top and bottom, except at very low densities. Since up and lower DN divertor magnetic topologies appear to be well balanced, this clearly demonstrates the role of classical drifts. Note, however, that the effect of drifts is sensitive to divertor and SOL plasma conditions [6, 13, 16]. Contrary to the above observations in the low power Ohmic discharges in EAST, the results obtained in DIII-D under H-mode plasmas shows that the peak particle flux at the upper divertor is higher than that at the lower divertor for well balanced DN for the normal B_T direction; this was attributed to the contribution from poloidal $\mathbf{E} \times \mathbf{B}$ drifts through the private flux region [14, 15, 17]. For DN Ohmic discharges in EAST, the plasma almost disappears at inner divertor targets (*e.g.*, see Figs 2, 4), therefore, it would be difficult to sustain such a poloidal $\mathbf{E} \times \mathbf{B}$ flow at the inboard divertor. In this case, the ion ∇B drift, whose polarity is in accordance with the experimental observations, appears to offer a plausible explanation. It is interesting to note that the j_s target distribution exhibits a multi-peak structure, which may be attributed to error fields on the outboard side. For SN, reversing the B_T direction leads to a further increase in the particle flux at the outer divertor target, most likely driven by $\mathbf{E} \times \mathbf{B}$ drifts through the private flux region. This triggers an abrupt transition to detachment at both outer and inner divertor targets, accompanied by a simultaneous increase in the core plasma radiation, ultimately reducing the density limit.

6. Divertor Screening for Impurities and Neutrals

The basic function of a divertor is to provide screening for impurities produced at at divertor target plates where strong plasma-surface interactions usually occur. Divertor screening for impurities predominantly relies on a strong flow naturally present in the divertor, which imposes a frictional drag on impurity ions and counteracts the ion temperature gradient force. The latter tends to drive impurity ions along the temperature gradient toward the main confinement chamber [13]. The efficiency of impurity screening is dependent on divertor geometry, impurity

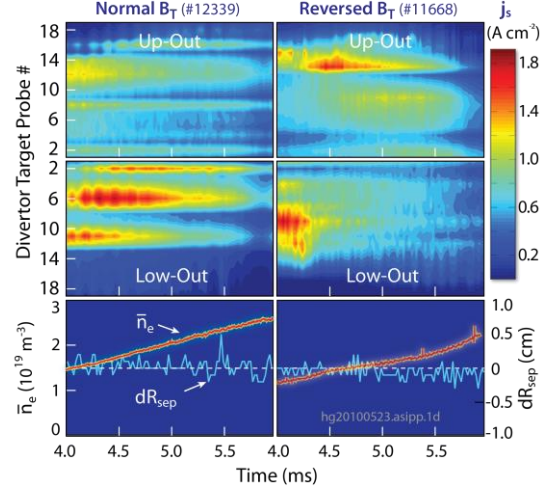


FIG. 5. Contours of j_s distributions on upper outer target and lower outer target for two DN discharges with normal and reversed B_T , respectively, and time traces of \bar{n}_e and dR_{sep} .

production mechanism and source distribution, as well as local plasma conditions [5, 18, 19]. It has been recently found that strong flows are also present in the SOL away from divertor targets, thus affecting impurity migration and divertor screening [20].

All plasma-facing components in EAST are covered with graphite tiles, so carbon is the dominant intrinsic impurity. For assessing divertor screening efficiency, a series of DN Ohmic discharges ($I_p = 250$ kA, $B_T = 2$ T) were carried out with a small amount of trace methane, CH_4 , being injected at various divertor locations, including outer divertor target, inner divertor target, and private flux region (dome). Figure 6 shows the time evolution of CIII measured at the outer midplane under different operating conditions. For low and intermediate densities, *i.e.*, $\bar{n}_e = 1.0 \times 10^{19} \text{ m}^{-3}$ and $1.5 \times 10^{19} \text{ m}^{-3}$, divertor exhibits strong screening for carbon with little changes in CIII intensity following the injection of CH_4 at all the divertor locations. By contrast, for the higher density case, *i.e.*, $\bar{n}_e = 2.0 \times 10^{19} \text{ m}^{-3}$, CH_4 puffing at the inner target, and especially the dome leads to a large increase in CIII, indicating relatively poor divertor screening for carbon sources from inner divertor target and private flux region. However, the change in CIII for outer target puffing remains similar to those for the low and intermediate density cases, as the outer divertor plasma is still in the high recycling regime or only partially detached, *e.g.* see Fig. 4. In this case, divertor plasma density and temperature remain sufficiently high, so that carbon can be ionized in the vicinity of divertor target plates where strong flow is present.

Localized D_2 puffing from various divertor locations has also been carried out on EAST to investigate divertor closure for neutrals and gas fuelling efficiency under typical Ohmic discharge conditions. Figure 7 shows the time evolution of line integrated electron density, $\int ndl$, with D_2 puffing at outer and inner divertor targets, as well as dome, for both DN and SN divertor configurations. As can be seen, D_2 puffing from the dome leads to a large increase in $\int ndl$ in both cases, suggesting strong leakage of neutrals from the private flux region. For the DN configuration, there appears to be a strong asymmetry in gas fuelling efficiency between inner

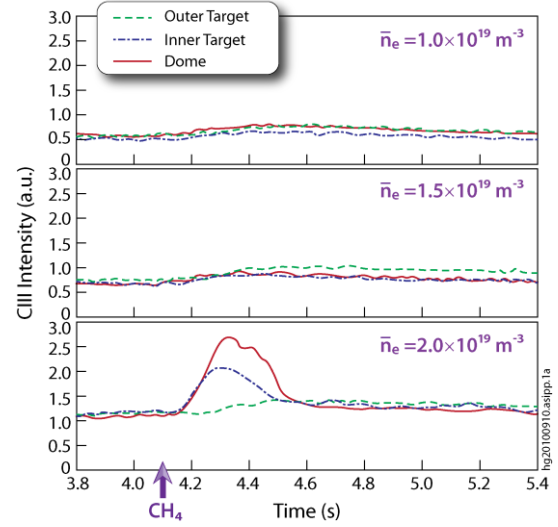


FIG. 6. Changes in CIII intensity with CH_4 puffing at outer target, inner target and private flux region (dome) in DN divertor plasmas at 3.63×10^{21} particles/s, starting at 4.1 s for 0.09 s.

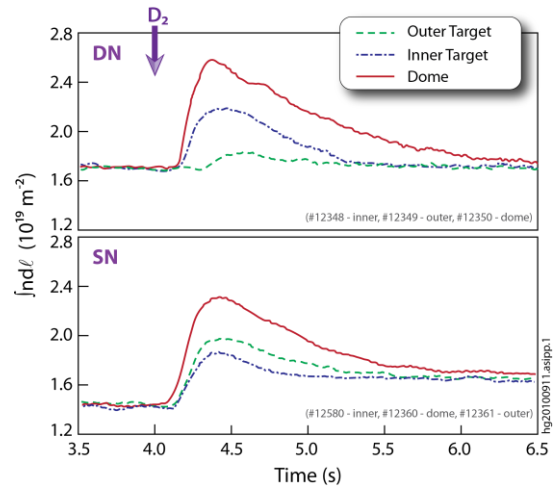


FIG. 7. Time evolution of line integrated density, $\int ndl$, with localized D_2 puffing at outer target, inner target and dome, for SN and DN Ohmic discharges with normal B_T .

and outer divertor gas puffing, with a significantly higher density rise following inner divertor puffing, thus indicating poor divertor closure for neutrals from the inner divertor target, presumably due to plasma detachment at the inner divertor target, as shown in Fig. 4. However, for SN, the gas fuelling efficiency appears to be similar between inner and outer divertor target gas puffing, resulting from similar plasma conditions in both inner and outer divertors.

7. Active Control of Divertor Target Heat Load by Ar Puffing

Divertor gas puffing offers an effective means for the control of divertor asymmetry and divertor target heat load [5, 21]. In particular, extrinsic high-Z impurity seeding has been used in many tokamaks to achieve partial or complete divertor detachment with strongly radiative divertor plasmas, which has been considered as a candidate for the control of target heat load in ITER [6].

First radiative divertor experiment was conducted on EAST in April 2009 by injecting the highly radiating recycling impurity Ar and deuterium mixture, *i.e.*, $D_2+5.7\%$ Ar, under steady Ohmic discharge conditions with active divertor pumping. Figure 8 shows the time evolution of an Ar seeded discharge with the Ar: D_2 mixture being simultaneously injected into the upper and lower outer divertor plasmas near the outer strike points for the DN configuration with the normal B_T direction. Gas puffing was initiated at 5s during the steady state phase of the discharge for duration of 0.3s at a puff rate of 8.19×10^{20} particles/s. This led to detachment at both upper and lower outer divertor targets, as indicated by j_s , significantly reducing the peak heat fluxes, q_{peak} , near outer strike points. It is remarkable that despite the presence of Ar, Z_{eff} in the core plasma is actually reduced, resulting from the increase in central plasma density.

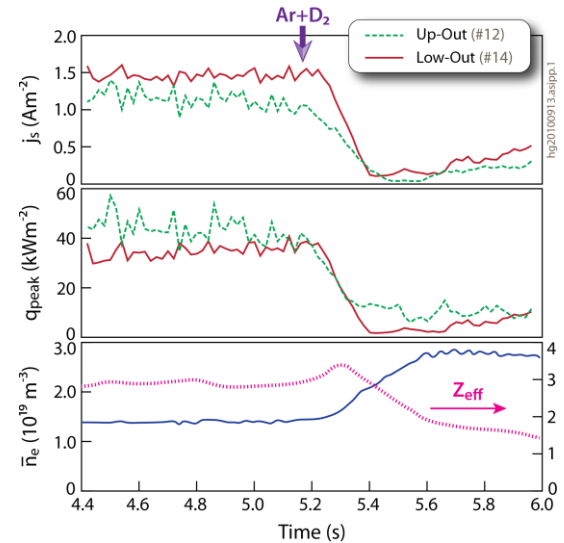


FIG. 8. Effect of Ar: D_2 mixture gas injection into upper and lower outer divertors for a typical double null Ohmic discharge with normal B_T .

8. Summary

First systematic assessment of the divertor performance was carried out on EAST under Ohmic and L-mode operating conditions, demonstrating partial detachment with $T_{et} \sim 3$ eV close to the strike point, as expected for the vertical target configuration. Detailed comparison between SN and DN configurations shows that particle and heat fluxes are similar at outboard divertor targets, but much lower at inboard divertor targets for DN. In addition, DN operation leads to an up-down asymmetry with a preferential particle flow in the $B \times \nabla B$ drift direction. Reversing the B_T direction mitigates or even reverses this up-down asymmetry, indicating strong contributions from ion ∇B drifts, while for SN, reversing the B_T direction leads to a further increase in the particle flux to the outer divertor target plate for the SN divertor configuration, most likely driven by the poloidal $E \times B$ drifts through the private flux region. This triggers an abrupt

transition to detachment at both outer and inner divertor target plates, accompanied by a simultaneous increase in the core radiation, ultimately reducing the density limit.

In addition, the divertor screening efficiency for carbon has been assessed for DN plasmas with CH₄ puffing, showing a strong dependence on divertor gas puff locations and local plasma conditions. Divertor screening is strong at low and intermediate densities, but is compromised at relatively high densities for methane injection at inner divertor target, and especially dome, as the inner divertor plasma approaches complete detachment. Localized divertor puffing of D₂ also shows poor divertor closure for neutrals from inner target and private flux region under similar DN operating conditions. Furthermore, Ar puffing has been explored as a means to mitigate in-out divertor asymmetry and reduce peak heat load at outer divertor target plates.

Acknowledgement

The authors want to acknowledge support from the rest of EAST Team. This work is funded by National Nature Science Foundation of China under contracts #10475078 and #10728510, and National Magnetic Confinement Fusion Program under contract #2010GB104000.

References

- [1] Wan, Y.X., et al., Nucl. Fusion **40** (2000) 1057.
- [2] BaonianWan, Nucl. Fusion **49** (2009) 104011.
- [3] Zhu, S., and Zha, X., J. Nucl. Mater. **313-316** (2003) 1020.
- [4] Guo, H.Y., Zhu, S., and Li, J., J. Nucl. Mater. **363-365** (2007) 162.
- [5] Loarte, A., Plasma Phys. Control. Fusion **43** (2001) R183.
- [6] Loarte, A., et al., Nucl. Fusion **47** (2007) S203.
- [7] Guo, H.Y., et al., "Recent Progress on Long Pulse Divertor Operation in EAST", to be published in J. Nucl. Mater. (Proc. 19th International Conference on Plasma-Surface Interactions in Controlled Fusion Devices, San Diego, May 24-28, 2010)
- [8] Wu, Z.W., et al., "First Study of EAST Divertor by Impurity Puffing", *ibid.*
- [9] Gao, W., et al., "Effect of Localized Gas Puffing on Divertor Plasma Behavior in EAST" *ibid.*
- [10] Xu, Q., et al., "Monte Carlo Simulation of Erosion and Deposition Behavior of SiC-coated Graphite Tiles in EAST", *ibid.*
- [11] Hu, Q.S., et al., "Particle exhaust and recycling control by active divertor pumping in EAST", *ibid.*
- [12] Tingfeng Ming et al., Fusion Engineering and Design **84** (2009) 57.
- [13] Stangeby, P.C., "The Plasma Boundary of Magnetic Fusion Devices" (IOP, Bristol, 2000)
- [14] Petrie, T.W., et al., J. Nucl. Mater. **290-293** (2001) 935.
- [15] Petrie, T.W., et al., J. Nucl. Mater. **313-316** (2003) 834.
- [16] Chankin, A.V., J. Nucl. Mater. **241-243** (1997) 199.
- [17] Porter, G.D., et al., J. Nucl. Mater. **313-316** (2003) 1085.
- [18] Guo, H.Y., et al., J. Nucl. Mater. **266-269** (1999) 825.
- [19] Guo, H.Y., et al., Nucl. Fusion **40** (2000) 379.
- [20] Matthews, G.F., J. Nucl. Mater. **337-339** (2005) 1.
- [21] Petrie, T.W., et al., Nucl. Fusion **37** (1997) 321.